Journal of Hydrology 608 (2022) 127672

Contents lists available at ScienceDirect

Journal of Hydrology

journal homepage: www.elsevier.com/locate/jhydrol

Research papers

# Season-specific evapotranspiration partitioning using dual water isotopes in a *Pinus yunnanensis* ecosystem, southwest China

Jiaojiao Han [a,b], Lide Tian [a,b,*], Zhongyin Cai [a,b], Wei Ren [a,c], Weiwei Liu [d], Jin Li [d], Jiangrong Tai [a,b]

[a] *Institute of International Rivers and Eco-Security, Yunnan University, Kunming, Yunnan 650500, China*
[b] *Yunnan Key Laboratory of International Rivers and Transboundary Eco-security, Kunming 650091, China*
[c] *Chongqing Jinfo Mountain Karst Ecosystem National Observation and Research Station, School of Geographical Sciences, Southwest University, Chongqing 400715, China*
[d] *Yunnan Lijiang Forest Ecosystem National Observation and Research Station, Kunming Institute of Botany, Chinese Academy of Sciences*

ARTICLE INFO

This manuscript was handled by Marco Borga, Editor-in-Chief, with the assistance of Yuting Yang, Associate Editor

*Keywords:*
Evapotranspiration partitioning
Water isotopes
Seasonality
Forest ecosystem
Southwest China

ABSTRACT

Quantifying the regional evapotranspiration is critical in terrestrial water balance and global water cycle, while partitioning of evapotranspiration is challenging but fundamental to predict the fate of terrestrial ecosystems under climate changes. Here, we performed in-situ measurements of water isotopes in atmospheric vapor, plant tissues and soil pools in a *Pinus yunnanensis* forest ecosystem in southwest China, aiming to partitioning ET by estimating the stable isotopic compositions of ET and that of its two components, i.e., plant transpiration and soil water evaporation. We used combined high-frequency laser spectroscopy and chamber methods, to constrain the estimates of T/ET. We first found that the estimated daily T/ET ratio ranges from 0.59 to 0.81, with an apparent increasing shift in the early growing season and maintaining a plateau level of over 0.75 during the peak growing season. This higher averaged T/ET of 0.73 ± 0.06 indicates that plant transpiration is the main component of evapotranspiration. The estimated $\delta_E$ and $\delta_T$ are in agreement with result from customized chamber method. We also found that in monsoon season (in June-September), soil water content is the main control of T/ET variations, with leaf area index playing only a partial role. Our study confirms the critical impact of soil water on the seasonal change of T/ET in *Pinus yunnanensis* ecosystem such as the SW China. However, we are also aware the sensitivity of controls on estimated T/ET at different time scale interested. Our results here provide insight into the regional hydrological cycle in alpine forest ecosystem and potentially benefits many applications from forest ecosystem protection to paleo isotope archives.

## 1. Introduction

Increasing stress from climate change exerted its impact on water cycle of the global terrestrial ecosystem, and hydrological cycle is expected to be intensified and to alter evapotranspiration (ET), with implications for feedback to regional and global climate (Jung et al., 2010). Evapotranspiration is the most important process that influences ecosystem water loss and a major determinant of the water budget and energy balance in the ecosystem. However, in the terrestrial water cycle budget, evapotranspiration determined by the intensities and relative proportions of evaporation from the soil (E) and transpiration through the stomata of plants (T), is still a major uncertainty, especially in the stress of climate change. Since T fluxes link the water and carbon cycles (Scott et al., 2006), it transfers a significant portion of water from the soil to the atmosphere with consequences for regional humidity and precipitation patterns (Aguiar et al., 1996; Kool et al., 2014; Prince et al., 1998). Therefore, quantitative estimation of T in the total ET (T/ET) has long been acknowledged to play a crucial role in water resource management, yield estimation, the water cycle and climate change, from plot scale to global scale (e.g., Jasechko et al., 2013; Kool et al., 2014). In addition, as water limited environments currently comprise about half of the earth's land surface and are expected to continue to expand (Newman et al., 2006), the issue of accurately assessing ET and its components has become more acute in recent studies in related to isotope hydrology, ecosystem processes and climate change (Dubbert et al., 2014; Jasechko et al., 2013; Jefferson et al., 2017; Zhang et al.,

* Corresponding author at: Institute of International Rivers and Eco-security, Yunnan University, Kunming, Yunnan 650500, China.
*E-mail address:* ldtian@ynu.edu.cn (L. Tian).

https://doi.org/10.1016/j.jhydrol.2022.127672
Received 30 November 2021; Received in revised form 21 January 2022; Accepted 26 February 2022
Available online 3 March 2022

2018). On a global scale, concerns about climate change have raised interest in the connection between ET and carbon sequestration (Scott et al., 2006), and the influence of ET partitioning on land–atmosphere patterns which affect climate simulations (Lawrence et al., 2007). Consequently, the topic of evapotranspiration partitioning has gained much attention in the scientific community (e.g., Berkelhammer et al., 2016; Lu et al., 2017).

At present, various methods have been developed for ET partitioning at different spatial and temporal scales (Coenders-Gerrits et al., 2014; Fatichi and Pappas, 2017; Scott and Biederman, 2017; Wei et al., 2017), such as those from field observations (Zhou et al., 2016), remote sensing model estimation (Miralles et al., 2016), process-based model simulations (Wang-Erlandsson et al., 2014) and reanalysis data (Kochendorfer and Ramírez, 2010). Isotopic measurements (Good et al., 2015) have been increasingly used to partition ET at these scales owning to the sensitivity of isotope fractionation in evaporation. The stable isotope method for ET partitioning is usually based on the principle of isotope mass balance; thus, the analysis of the water stable isotopic compositions within soil, vegetation and the atmosphere are the core issue (Xiao et al., 2018).

In spite of the ET partitioning efforts over the past decades, there is a significant discrepancy among global T/ET estimated by different methods and large uncertainty still exists at different spatial–temporal coverages. At the global scale, the magnitude of T/ET differs substantially (20%–90%) among different methods (Coenders-Gerrits et al., 2014; Jasechko et al., 2013; Good et al., 2015; Maxwell and Condon, 2016; Miralles et al., 2016; Wei et al., 2017). The distinct isotope effects of T and E showed that T represents 80–90% of terrestrial ET at basin and global scales by using a combination of isotope measurement techniques and satellite observations (Jasechko et al., 2013). Such high ratio was questioned and challenged by following correspondence (Schlesinger and Jasechko, 2014; Coenders-Gerrits et al., 2014). Lately, Good et al. (2015) adjusted the global T/ET ratio to 64 ± 13% by using the satellite isotope data and large-scale water balance method. Wei et al. (2017) modified the global T/ET to be about 57% with a leaf area index (LAI)-based ET partitioning algorithm. The uncertainty is likely persistent since plot scale ET partitioning observations at relevant spatiotemporal scales for large scale T/ET upscaling (Wei et al., 2017), constraint (Lian et al., 2018) and validation (Rigden et al., 2018) are still lack.

At plot scale, isotopic methods have been widely used for ET partitioning at different ecosystem, including forests (Dubbert et al., 2013), savanna (Yepez et al., 2003), grassland (Good et al., 2014) and farmland (Wei et al., 2015) for the past two decades. The main effect involved is to determine the environment factors that controls T/ET changes, which is necessary for better upscaling hydrological cycling to large areas (Wei et al., 2017), as well as land-surface modeling (Ma et al., 2017).

Forest ecosystems cover approximately 30% of the Earth's land surface (Hansen et al, 2014) and play an essential ecological role in the earth-atmosphere interaction, the earth's surface energy balance and hydrological cycle. The alpine forest exerts a strong regulating function on preventing soil erosion and regulating climate system (Altieri et al, 2018). Many previous effects have addressed the water cycle in association with the forest ecosystem, with a specification on ET participation. By using the STEAM Model, Wang-Erlandsson et al. (2014) simulated the global ET and its components and found that deciduous broadleaved forest had the largest T/ET value (0.64), and evergreen coniferous forests had the smallest value (0.50). Liu et al. (2020) used eddy covariance technique and sap-flow probes and concluded that the overall T/ET varies in the range of 0.66–0.84 in a larch forest in most northern China. However, previous studies have focused mainly on lower elevations or only estimated the gross evapotranspiration, and a gap exists in the study of seasonal evapotranspiration processes and its controlling factors in alpine forest ecosystems.

Stress increased in recent years to protect the forest ecosystem in southwest China due to their ecological importance, characterized by ecological security barrier and vulnerable global climate change. Coniferous-leaved forests are one of the wide transcontinental distribution and keystone forest types in subalpine forest ecosystem. Here, we reported a new result on isotope-based land surface water cycle in a typical subalpine forest region in Lijiang, Yunnan-Guizhou Plateau in southwest China, by employing a high-frequency laser spectrometry and chamber method throughout an entire raining season. We made continuous measurement of isotopes in atmospheric vapor and evapotranspiration in the raining season (June to September) of 2019. $\delta_E$ and $\delta_T$ were directly measured by newly customized chambers, or calculated from commonly used non-process-based empirical models (Keeling plot, Craig-Gordon model and isotopic steady-state assumption). The paper aims, first, to determine the seasonal shift of water isotope in different water bodies and water transfers among precipitation, soil water, xylem water, then to evaluate the variations of E, T and ET in *Pinus yunnanensis* forest ecosystem, and partition evapotranspiration into transpiration and evaporation for an improved understanding of the dynamics that drive the seasonal variations of T/ET.

## 2. Materials and methods

### 2.1. Site description

We made observation of water isotopes in precipitation, plant, soil water and atmospheric vapor at Lijiang Forest Ecosystem Research Station (100°10′E, 27°00′N; 3250 m above sea level) at the southern edge of a Yulong Mountain, southwest China. Yulong Mountain is recognized as the southern boundary that alpine glaciers can survive in the Asia monsoon region and these glaciers are extremely sensitive to climate change (He et al., 2002). This region belongs to the Hengduan Mountains region and is located in the southeastern margin of the Qinghai-Tibet Plateau, known as the center of the Mountains of Southwest China biodiversity hotspot.

The region is featured with a high-altitude monsoon climate, with Indian monsoon intrusion in summer and persistent westerly jet in winter. The average annual precipitation is 935 mm, with distinctive seasonality of over 90% of the annual precipitation in summer from June to September, while little precipitation in dry winter season from October to next May (Niu et al., 2013). The monthly air temperature varies from 5.9 °C in January to 17.9 °C in July, with annual average of 12.8 °C based on data from Lijiang Meteorological Station (Feng et al., 2006). The overlying soil in a Yulong Snow Mountain is loam and clay according to the FAO soil classification. The vertical vegetation zonation is obvious with elevational gradient in Yulong Mountain. At the lowest elevation (2650 m), the forest vegetation is dominated by *Pinus armandii*. At 2950 m, the forest vegetation shifts to the dominated evergreen conifers *P. armandii* and *Pinus yunnanensis*, and the sclerophyllous evergreen broad-leaved *Quercus spinosa*, forming a mixed coniferous/sclerophyllous broad-leaved forest. Above 3250 m, the forest vegetation is dominated by *Quercus guyavifolia* and *P.yunnanensis*. At the highest elevation (3850 m) the forest composition is dominated by *Quercus aquifolioides*, *Abies georgei* and *Rhododendron rubiginosum* (Luo et al., 2016). The annual average evapotranspiration of the subalpine coniferous forest is 438.83 mm, accounting for 42.17% of the annual precipitation in the ecosystem, and the maximum occurs in wet season (Lin et al., 2019). In this paper, we selected *Pinus yunnanensis* as the target tree for transpiration observation by water isotope approach. The height of the community varies from 5 m to 10 m in the sampling plot. In this study, the growing season is defined as the period from May to September.

### 2.2. Sampling and measurement

We performed continuous monitoring of water isotopes in atmospheric vapor, soil water, xylem water, leaf water simultaneously during May to September of 2019. We also collected precipitation for isotope

measurement as input water isotope signal during the same period. Following we made description on how we made the monitoring and sampling work at the experiment plot.

#### 2.2.1. Vapor isotope measurement

We used a Picarro L2130-i high frequency wavelength scanning cavity decay spectrum analyzer for atmospheric vapor isotope measurement. The analyzer is placed in room on the site to ensure the stability of the ambient air temperature. Two models (i.e., solid model and vapor model) were switched to measure water isotopes in plant and soil water samples (Cui et al., 2017), or the near surface water vapor (Steen-Larsen et al., 2013). In vapor mode, the measurement and calibration system are comprised of a standard delivery module A0101, a vaporizer module A0211 (Picarro Inc., Santa Clara, CA), and an analyzer. The schematic diagram, working principle and calibration process of the CRDS analyzer was described elsewhere (Wang and Dickinson, 2012). In practice, instrumental drifts and humidity dependence of water vapor isotopes were corrected before normalizing to V-SMOW scale, and calibration measurement was performed every 12 h following the protocols of Steen-Larsen et al. (2013). We measured the atmospheric vapor isotopes at 8 layers along a vertical profile of 0.5, 1, 2, 3, 5, 10, 15 and 20 m above the ground, utilizing eight-way solenoid valves and from 13:00–15:00 and 23:00-next 8:00 h (local standard time, UTC + 8) every day. Each level was measured for 10 min during the noon hours from 13:00–15:00 and the average of the last 5min was used to establish the Keeling plot to obtain $\delta_{ET}$. Since soil water and plant water isotopes were measured in daytime using the same isotope analyzer, the vapor isotope measurement was intermittent in daytime. The precision was 0.2‰ for vapor $\delta^{18}O$ and 0.5 ‰ for vapor $\delta^{2}H$.

#### 2.2.2. Plant and soil water sampling and isotope measurement

Soil water, xylem water and leaf water were measured at 13:00 to 15:00 every other day, and three duplicated samples were measured each time and the average value is used for representative. A total number of 362, 47 and 47 samples of soil water, xylem water and leaf water were collected for isotope analysis. Occasional samples were also collected after raining events, to reveal the direct raining impact on soil and xylem water isotopes. In each measurement, the collected xylem samples from the base of the plant (green tissue, e.g., outer leaf) were stripped and only the white (i.e., non-transpiring) tissue was used for measurement. We measured plant samples at different sides of the tree (east, west, south, north) and from three mature trees for the representative of the measurement. Soil samples were collected at depth of 5 cm, 10 cm, 20 cm, 30 cm, 50 cm and 80 cm at each time, with a hand drill at sites near the three trees. Plant xylem (*Pinus yunnanensis*) and soil samples were measured by the isotope analyzer in solid mode combined with an induction module (IM). The solid mode allowed for the simultaneous measurement of the isotopic compositions of small solid samples and the removal of organic contamination from within the samples in the field (Quade et al., 2019). The measurement of the plant and soil water immediately after sampling will also reduce the influence of evaporation on water isotopes. Three laboratory standard waters were used for calibration: $S_1$ ($\delta^{18}O$ = -2.83‰, $\delta^{2}H$ = -27.42‰), $S_2$ ($\delta^{18}O$ = -29.84‰, $\delta^{2}H$ = –222.84‰) and $S_3$ ($\delta^{18}O$ = -15.29‰, $\delta^{2}H$ = -110.30‰), which roughly cover the ranges of the measured water isotope ratios. For the measurement procedure, 3 μL of laboratory standard water ($S_1$ and $S_3$) was injected onto glass filter paper (Whatman plc, Maidstone, UK) for calibration prior to sample measurements. Xylem samples were wrapped in small tri-fold metal strips (Picarro Inc., Santa Clara, CA) and placed inside a 4 mL glass vial. The vial was inserted into the IM and heated through induction and the evaporated vapor was sent to analyzer for isotope measurement. For soil samples, each soil sample (~4μg) was put into a steel pipe (Picarro Inc., Santa Clara, CA) with 20 mm in length and 5 mm in diameter and also placed inside a vial. This process generally required 5 min to measure for one xylem sample, and 10 ~ 15 min to measure for one soil water sample. The measured precision is ± 0.20 ‰ for $\delta^{18}O$ and ± 0.69‰ for $\delta^{2}H$. The detailed measurement and calibration processes followed the protocol of Cui et al. (2017).

#### 2.2.3. Precipitation sampling and measurement

We used two methods to collect precipitation samples. Daily precipitation samples were collected at 20:00 in the raining day using a container, specifically designed to avoid re-evaporation of collected water samples. In addition, 170 precipitation event samples were collected in the period from May to September 2019. All samples were stored in plastic bottles and frozen in refrigerator before laboratory analysis. The collected precipitation samples were analyzed in laboratory by using Picarro L2140-i liquid water isotope analyzer for both $\delta^{18}O$ and $\delta^{2}H$. All measured results were normalized to VSMOW (Vienna Standard Mean Ocean Water), with precision within ± 0.05‰ for $\delta^{18}O$ and ± 0.5‰ for $\delta^{2}H$.

### 2.3. Micrometeorological and eddy covariance measurements

We installed the eddy covariance (EC) instruments meteorology station at the sampling station, including an open path infrared $CO_2$/$H_2O$ gas analyzer (Li-7500 A, Li-Cor, USA) and a three-dimensional sonic anemometer thermometer (CSAT3, Campbell Scientific Inc., USA) mounted 3 m above the ground. The data were stored in a CR6 data logger and CF storage card at a sampling frequency of 10 Hz. The Raw data acquired at 10 Hz were processed using the postprocessing software EdiRe, and quality control of the half-hourly flux data were conducted as described in earlier literature (Xu et al., 2013) and will only be summarized here. Micrometeorological parameters (air temperature, relative humidity, wind speed, precipitation amount, four-component radiation, three layers of soil temperature and soil moisture profiles, soil heat flux, etc.) were recorded under 1 Hz. Additional details concerning data acquisition were described (Liu and Zhang. 2012; Eichelmann et al., 2018). Based on measurements from the EC system, the energy balance closure ratio was evaluated at this site, and result shows a relatively high energy balance closure ratio of 0.88, indicating that the energy balance closure problem (Wilson et al., 2001) is not a major concern for the site and system. Leaf area index (LAI, 1-hour composited, 0.25°) data from the ERA-5 product were used in the discussion about the control of seasonal T/ET ratio. The values proved to be broadly consistent with observations. Data were downloaded from the European Centre for Medium-Range Weather Forecasts (https://www.ecmwf.int/).

### 2.4. Methods

#### 2.4.1. Isotopic flux partitioning

Water stable isotopes have been widely used to estimate plot-scale ET partitioning (Yepez et al., 2003; Good et al., 2014; Wei et al., 2018) owing to the distinctive isotope signal of $\delta_{ET}$, $\delta_E$ and $\delta_T$ resulted from deviated fractionation between evaporation and transpiration. Utilizing a two end-member (E and T) mixing model, the partitioning can be expressed as the three isotope signals by the following equation (Yakir and Sternberg, 2000):

$$\frac{T}{ET} = \frac{\delta_{ET} - \delta_E}{\delta_T - \delta_E} \quad (1)$$

where $\delta_{ET}$, $\delta_E$ and $\delta_T$ are isotopic compositions of evapotranspiration (ET), soil evaporation (E) and plant transpiration (T), respectively. This equation requires that the isotopic ratio of the ET, E and T fluxes to be known for model estimation.

#### 2.4.2. Isotopic composition of soil evaporation

Considering both equilibrium and kinetic fractionation during the phased change of water from liquid to vapor, the Craig-Gordon Model (Craig and Gordon, 1965) is the most common method widely employed

for estimating $\delta_E$, and has been successfully applied under different conditions (Yepez et al., 2003; Rothfuss et al., 2010; Good et al., 2014; Wei et al., 2015; Xiao et al., 2018). Using the isotopic composition of soil water at the evaporating surface ($\delta_S$) and vapor measured at the reference height ($\delta_V$) as well as various meteorological variables, $\delta_E$ can be calculated as follows:

$$\delta_E = \frac{\alpha_e^{-1}\delta_S - h^*\delta_V - \varepsilon_{eq} - (1-h^*)\varepsilon_k}{(1-h^*) + 10^{-3}(1-h^*)\varepsilon_k} \quad (2)$$

where $\alpha_e$ (>1) is the equilibrium fractionation factor calculated as a function of water surface temperature (Majoube, 1971), $\varepsilon_{eq} = (1-1/\alpha_e) \times 10^3$(‰) represents the equilibrium fractionation effect, $\varepsilon_k$ is the isotopic kinetic fractionation effect. If the diffusion is molecular, then $\varepsilon_k$ of $\delta^{18}O$ is equal to 28 ‰ (Merlivat, 1978). $h^*$ is the relative humidity normalized to the surface soil temperature (Craig and Gordon, 1965).

#### 2.4.3. Isotopic composition of plant transpiration

Isotope mass conservation requires that the isotopic composition of leaf transpiration water should be equal to that of soil water absorbed by roots at midday and in the early afternoon when ET is most intensive, commonly known as the "isotope stable state" hypothesis (ISS) (Yakir and Sternberg, 2000). We assumed that $\delta_T$ is equal to the isotope values of plant water source under ISS (Xiao et al., 2012). Under the premise of ISS, the isotope values of unfractionated water in the xylem can be used as substitute of the isotopic signal of transpiration water vapor. Hence, we assume the water leaving the leaf has the same isotope composition as the xylem water (Dawson and Ehleringer, 1993), then we have:

$$\delta_T = \delta_x \quad (3)$$

where $\delta_x$ is the isotopic ratio of xylem water, and $\delta_T$ is the isotopic ratio of transpiration.

#### 2.4.4. Estimation of the isotopic composition of evapotranspiration

A direct measurement of $\delta_{ET}$ in forest is difficult. Here we acquire $\delta_{ET}$ from the intercept of the linear regression of atmospheric vapor $\delta_a$ with the inverse of the vapor mixing ratio measured across multiple heights over a specific time interval (Keeling, 1958):

$$\delta_a = \frac{1}{C_a}\left[C_{bg}\left(\delta_{bg} - \delta_{ET}\right)\right] + \delta_{ET} \quad (4)$$

where $C_{bg}$ and $\delta_{bg}$ are the mixing ratio and isotopic composition of the background (i.e., local) atmospheric vapor. It is assumed that $\delta_{ET}$ and $\delta_{bg}$ remain constant over the course of observations. The threshold value of $R^2$ in the Keeling plot is 0.80 in this study (Fig. A1).

#### 2.4.5. Chamber-based measurements of $\delta_T$ and $\delta_E$

Recently, the chamber method was introduced to directly measure $\delta_T$ (Wang et al., 2010; Dubbert et al., 2014) and $\delta_E$ (Dubbert et al., 2013; Lu et al., 2017), with the development of high-frequency laser spectroscopy. The major advantage of the chamber method is that it offers an alternative solution to estimating $\delta_{ET}$, $\delta_E$ or $\delta_T$ without the use of complex isotopic models. Here two kinds of transparent cylindrical acrylic chambers were developed to measure $\delta_T$ and $\delta_E$ of the alpine forest ecosystem following the methods described by Wang et al. (2012).

For $\delta_T$, the chamber is made of two half cylinders (Teflon lined transparent plastic) that joined at a neoprene gasket, allowing for leaf samples to be placed inside the chamber while still connected to plant xylem. The base plate of the chamber was removed and a 1/4′ brass bulkhead was installed to allow the isotope analyzer inlet to connect the chamber base. Two small air vents at the base are the only path that allow the ambient air to enter the chamber and mix with water vapor transpired by the leaves. The mixed vapor was finally pumped to the analyzer through a 3-m long and 1/8″ inner diameter tube (consisting of a 0.5-m Teflon tube and a 2.5-m stainless steel tube) for isotopic analysis. The residence time of vapor in the tube (total volume: 150 $cm^3$) is only 18 s at a flow rate of 500 $cm^3$/min, which is negligible in terms of the chamber measurement. Furthermore, to exclude the influence of residual vapor from previous measurements in the tube, a break of ~ 2–3 min was set between two subsequent measurements to guarantee that vapor concentration dropped back to background level before the next measurement.

For $\delta_E$ measurement, a cap was directly placed on areas with bare soil. The cap was tightly covered on the ground to seal the chamber. This procedure ensures that only soil evaporation vapor ($\delta_E$), as mixed with ambient air from air vents on the cap, is measured by the analyzer. The specifics of the chamber have been reported elsewhere (Cui et al., 2020). In practice, we first measured the ambient vapor isotopes for 2 min. Then we closed the chamber and made measurement of the mixed water vapor for another 2 min. Since the concentration and isotopic composition of water vapor in the chamber reached a steady state (showed little change with time) after ~ 1–1.5 min, we ignored the measured result for the first 1.5 min, and only used the average results for the last 0.5 min as the measured $\delta_E$. This method provided, respectively, ambient and steady-state values to calculate the two end members. Based on isotope and water mass balance, the isotopic composition of source water vapor, $\delta$ ($\delta_T$, or $\delta_E$), was calculated as (Dubbert et al., 2014):

$$\delta = \frac{C_M\delta_M - C_A\delta_A}{C_M - C_A} \quad (5)$$

where $\delta$ is the isotopic composition of source water vapor (e.g., plant transpired water or evaporation), $C_A$ and $C_M$ are the concentrations of ambient and mixed water vapor in the chamber [mol $m^{-3}$], and $\delta_A$ and $\delta_M$ are the isotopic compositions of ambient and mixed water vapor in the chamber at the steady state.

## 3. Results

### 3.1. Seasonal variations of meteorological and biotic variables

Detailed information on the seasonality of the environmental variables is essential to assess seasonal variations in ET (Zhu et al. 2013). Fig. 2 shows the seasonal variations of daily air temperature (Ta), relative humidity (RH), net radiation (Rn), wind speed (u), daily precipitation amount (P) and half-hour average of volumetric soil water content (Swc) at different depth from the in-situ flux observation. Daily air temperature varies in the range of 6.8–18.6 °C (Fig. 2a). Daily wind speed is 0.5 m $s^{-1}$ in the monitoring period, varying from 0.2 to 1.3 m $s^{-1}$ (Fig. 2b). Mean net radiation varied between 15.9 and 199.9 W $m^{-2}$ (Fig. 2b), and daily average precipitation was 10.6 mm $d^{-1}$. The soil moisture content is quite constant in deep layers, and slight variations is in response to precipitation events but with lag of a couple of days.

### 3.2. Relationship between $\delta^{18}O$ and $\delta^2H$ of different water

To provide context for interpreting the nearly continuous measurements of $\delta_{ET}$, we first present the measurements of the liquid water pools (Fig. 3). We compared the $\delta^2H$-$\delta^{18}O$ relations in different water samples (precipitation, soil water, xylem and leaf water) with the global meteoric water line (GMWL) (Craig, 1961) (Fig. 3). The local meteoric water line (LMWL), $\delta^2H = 8.07\ \delta^{18}O + 10.52$ ($R^2 = 0.99$, $p < 0.001$, n = 80) (Fig. 3), is very close to the global meteoric water line of $\delta^2H = 8.17\ \delta^{18}O + 10.56$ (Rozanski et al., 1993). The variation of $\delta^{18}O$ and $\delta^2H$ in the soil water ranged from −5.3‰ to −21.3‰ and from −60.6‰ to −165.8‰, with mean values of −15.3‰ and −119.6‰, respectively. Soil water isotope signatures are mainly scattered in the lower of the LMWL as soil water is more a signal of weighted average of precipitation. The soil water line (SWL) equation is $\delta^2H = 7.12\delta^{18}O - 12.17$ ($R^2 = 0.88$, $p < 0.001$, n = 362), with lower slope and intercept than the

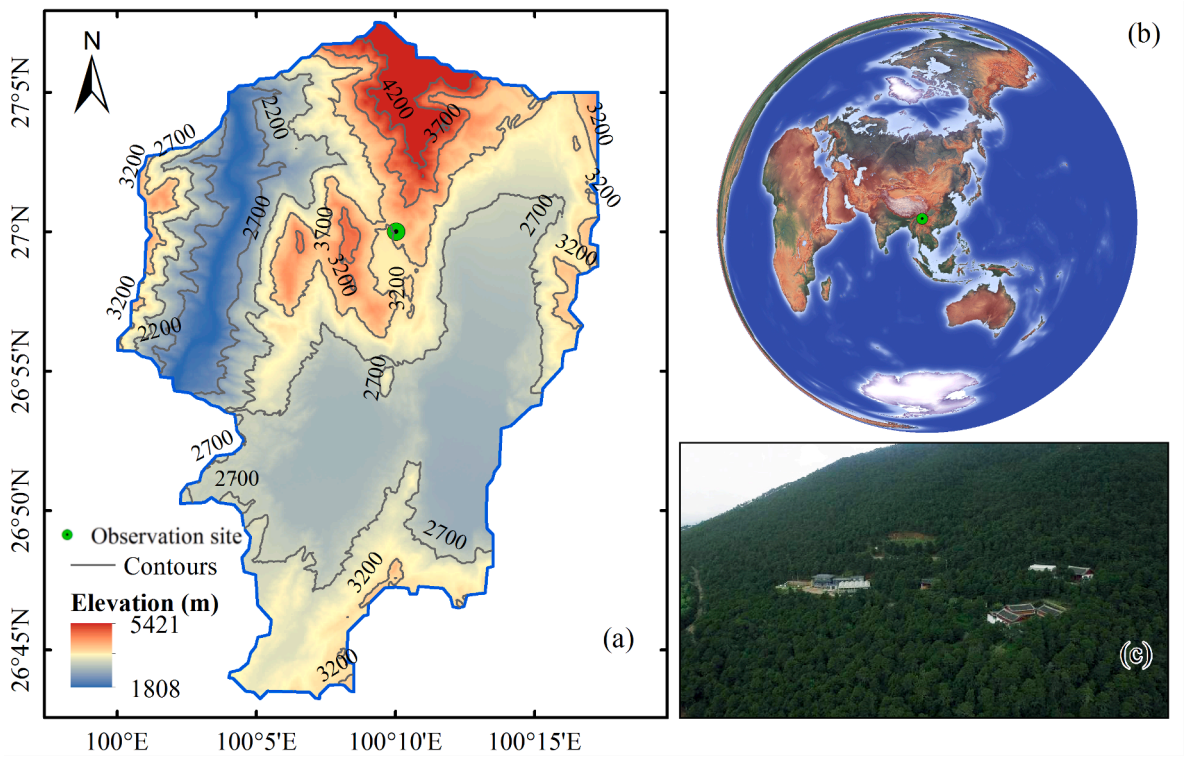


**Fig. 1.** The geographic sitting of the Lijiang station (a), its location (marked by a green circle) in the Yunnan-Guizhou Plateau (b) and a photo of the landscape at the observation site (c).

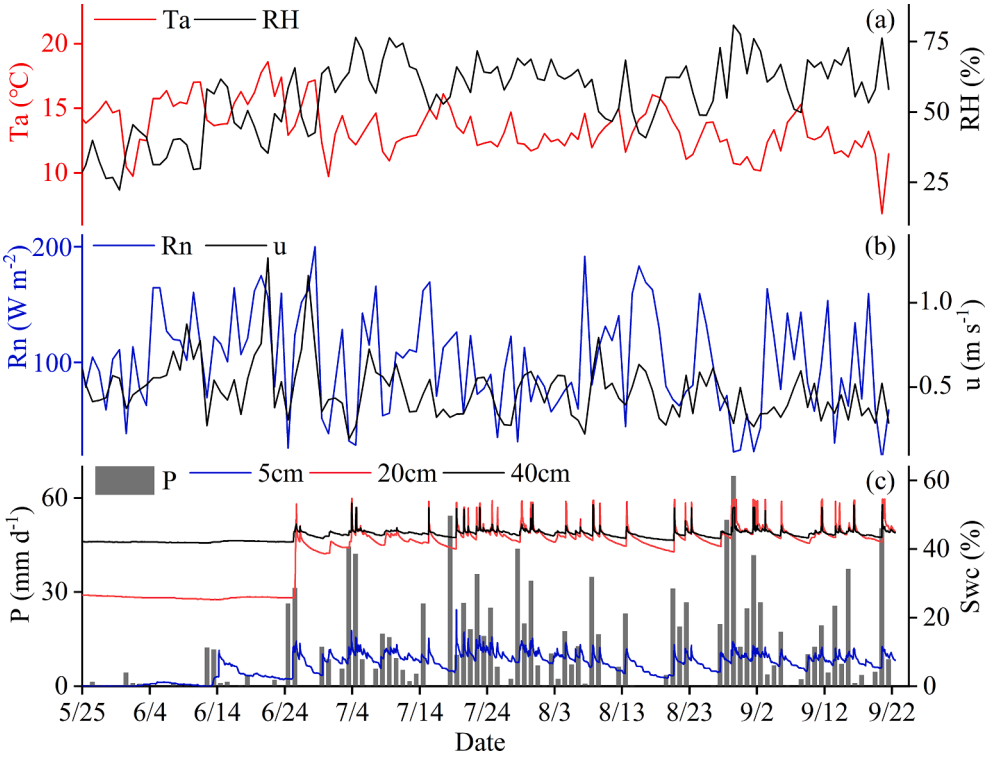


**Fig. 2.** Seasonal variations in (a) daily mean temperature (Ta) and relative humidity (RH); (b) net radiation (Rn) and wind speed (u); and (c) daily precipitation amount (P) and half-hour average of volumetric soil water content (Swc) at 5cm depth (blue line), 20 cm depth (red line) and 40 cm depth (black line) during the observations.

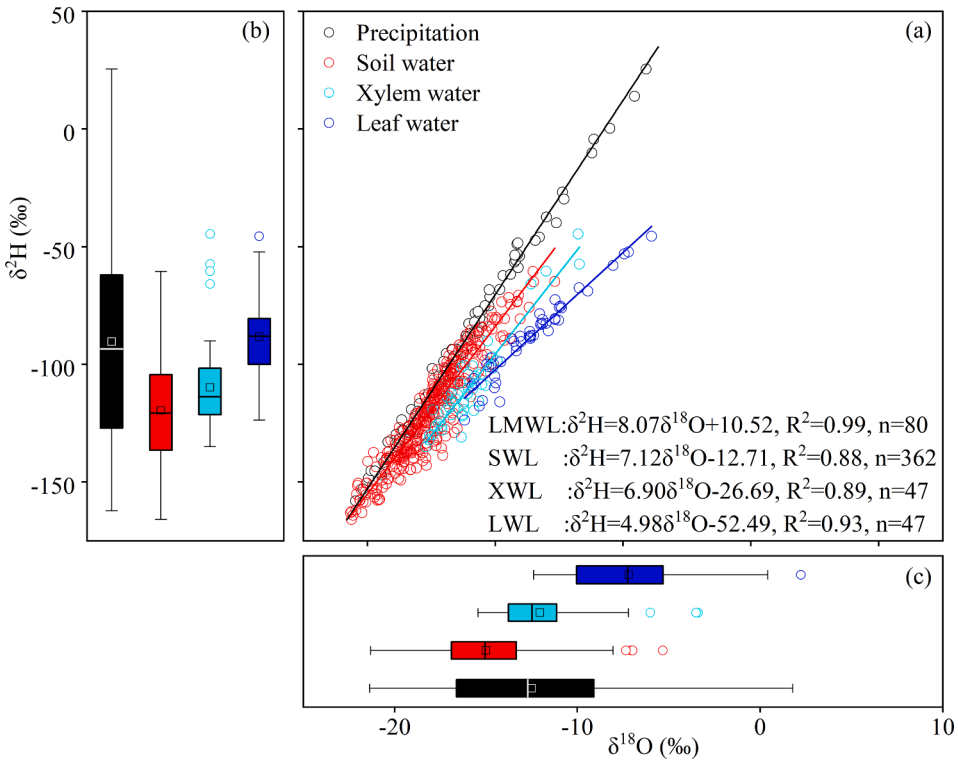


**Fig. 3.** Relationship between $\delta^{18}O$ and $\delta^{2}H$ in precipitation (open black circles), soil water (red black circles), xylem water (open green circles) and leaf water (open blue circles). (a) and (b) are the $\delta^{18}O$ and $\delta^{2}H$ of different water bodies, respectively, and (c) is the linear regression line of $\delta^{18}O$ and $\delta^{2}H$ in different water pools. The box indicates the 25th and 75th percentiles with the median as thick black line and the average as square. The error bars indicate the minimum and maximum values. The circles indicate outliers (3/2 times the central box).

LMWL owning to the slight evaporation of soil water in storage after rainfall. The equation of the plant xylem water line (XWL) is $\delta^{2}H = 6.90\delta^{18}O$ -26.69 ($R^2 = 0.89$, $p < 0.001$, n = 47), roughly parallel with the soil water line but with a more negative intercept due to the selective absorption of soil water at different levels.

We also identified a leaf water evaporation line (LWL) of $\delta^{2}H = 4.98\delta^{18}O$ -52.49 ($R^2 = 0.93$, $p < 0.001$, n = 47), specifically for the *Pinus yunnanensis* in this alpine forest ecosystem. The leaf water line is significantly lower in slope than in xylem water in association with the fractionation in leaf transpiration, with a slight seasonal shift between pre-monsoon season and monsoon season in association with the distinctive humidity change between the two seasons (Fig. A1).

### 3.3. Seasonal and diurnal variations of atmospheric vapor isotopes

The surface water vapor $\delta^{18}O$ flux ($\delta_V$) is a quantity frequently used to constrain the seasonal, diurnal and synoptic variability in the regional water cycle. We presented the in-situ measured daily $\delta^{18}O$ and $H_2O$ concentration of atmospheric vapor at 0.3m, 1m, 2m, 3m, 5m, 10m, 15m, 20m above ground (Fig. 4) (not continuously measured above 3.0m). The strong seasonality of vapor isotope is in association with the Indian summer intrusion from early June, with incidental increase of

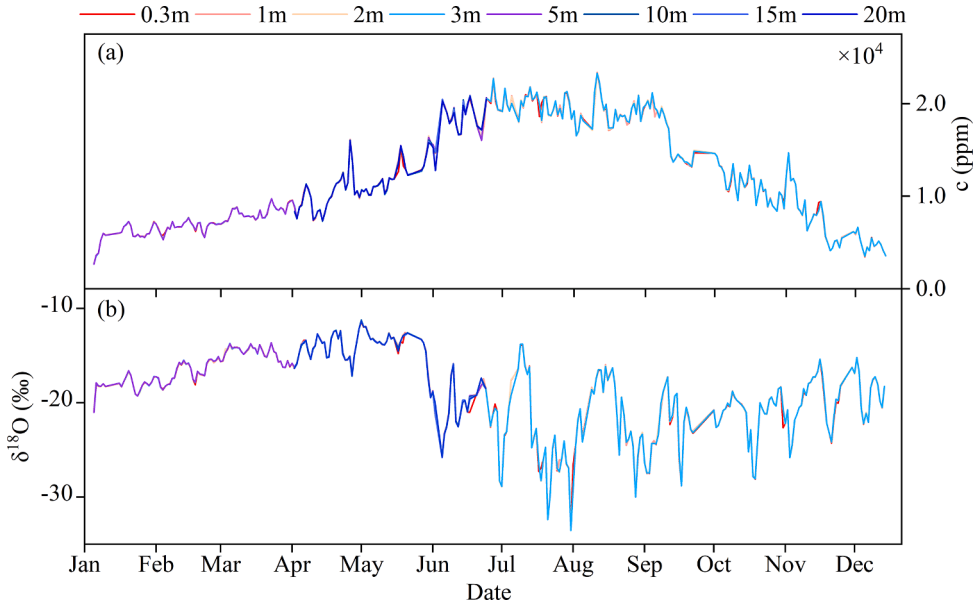


**Fig. 4.** Temporal variation of daily atmospheric water vapor $H^2O$ mixing ratio (a) and $\delta^{18}O$ (b) at Lijiang. The data of 0.3 m-3 m is from January to December 2019, the data of 5 m is only from January to July 2019, and the data of 10 m-20 m is only from April to July 2019.

vapor mixing ratio. The fluctuation of vapor isotope is lower in the non-monsoon season, but with large fluctuations in summer monsoon season owning to the local precipitation events. Both vapor isotopes and vapor mixing ratio show consistent change in different levels above ground.

Since the canopy height of the study area is 5-10m, while the continuously measured vapor isotopes are only available in 3.0 meter and below, therefore, we made a precise comparison of vapor isotopes and vapor mixing ratio in the spring season (April to July) when all level of measurement are available (Table A2). We see that the isotopes in different level are almost identical until to 20m (Fig. 4). Vapor mixing ratio show slight variation from ground to higher level, with general decrease trend above 2m level.

In the calculation of isotopes in evapotranspiration, we used the midday vapor isotope data instead of daily average. Hence, we also evaluated the diurnal change of vapor isotope at the sampling site. The 24 h ensemble average values of the vapor $\delta^{18}O$ at 3 m height measured from 13 to 16 October 2019 in non-raining days (Fig. A3). The overall diurnal change of vapor $\delta^{18}O$ is smaller, within 2‰ in all the four days.

### 3.4. Seasonal precipitation isotopes in the forest ecosystem

We presented the daily precipitation $\delta^{18}O$, d-excess and precipitation amount from Lijiang station (Fig. 5). Precipitation $\delta^{18}O$ shows a seasonal shift from the higher value in the earlier summer of May-June to the lower $\delta^{18}O$ period of the raining season until to September. This seasonal precipitation is consistent with the seasonal feature of monsoon type precipitation signal. Daily $\delta^{18}O$ values ranged from -21.4 ‰ to 1.8 ‰, with a weighted mean value of -13.0‰. The d-excess values ranged from -1.3 ‰ to 17.6 ‰, with a weighted mean of 10.9‰. Slight lower precipitation d-excess in less rainfall days are probably related to the reevaporation of falling raindrops, which lowered d-excess in the left rainfall.

### 3.5. Seasonal variation of the three flux endmembers ($\delta_E$, $\delta_T$ and $\delta_{ET}$)

Based on the observed vapor $\delta^{18}O$ together with the concurrent meteorological observation, we calculated the isotopic compositions of evaporation ($\delta_E$), transpiration ($\delta_T$) and evapotranspiration ($\delta_{ET}$) every other day using the methods descripted in the earlier section. Fig. 6 shows the seasonal $\delta^{18}O$ variations of $\delta_E$, $\delta_T$, and $\delta_{ET}$ during early afternoon hours (13:00-15:00) in the observation days. We also presented the daily precipitation $\delta^{18}O$ variations to discuss their linkage (Fig. 6).

On average, $\delta_T$ is 2.8‰ higher than $\delta_{ET}$, and 10.4‰ higher than $\delta_E$. Three of them show parallel temporal variations, with the largest magnitude in $\delta_E$ variation, indicating the conherent influence on the seasonal variations of the three. A comparison with daily precipitation isotope demonstrates that precipitation strongly impact the temporal variation of $\delta_E$, $\delta_T$ and $\delta_{ET}$. Correlation analysis also shows the significant relationship between the three end members and precipitation $\delta^{18}O$ ($R^2 = 0.85, 0.55, 0.83$, $p < 0.001$, respectively) suggest that the former was strongly affected by precipitation isotopes.

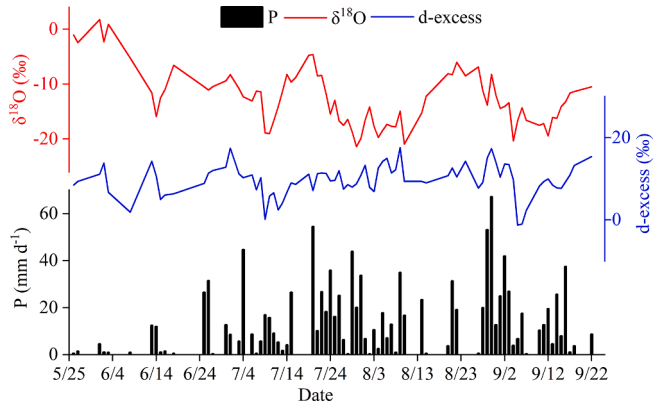


**Fig. 5.** Daily precipitation $\delta^{18}O$ and d-excess as comparison with precipitation amount.

### 3.6. Seasonal propagation of T/ET estimation in forest ecosystem

We calculated the relative contribution of T to ET (T/ET) based on the Keeling-CG method, by using both $\delta^{18}O$ and $\delta^{2}H$ measured in midday periods. The temporal variations of estimated T/ET from the dual isotopes are presented in Fig. 8. We also made the averaged T/ET from the two isotopes for a robust estimation of the seasonal characters and plotted in Fig. 7 as well. Results show a strong seasonal T/ET cycle, varying between 0.59-0.81. In the pre-monsoon season of June, the T/ET ratio shows a strong increasing trend, rising from 0.5 to 0.7. In the monsoon season, the T/ET ratio is higher with slight fluctuation of around 0.7-0.8. In average, the calculated ratio from $\delta^{18}O$-based method is identical with the $\delta^{2}H$-based results, yet there is a slight bias between the two with time. The average T/ET is 0.73 from isotopic labeling, indicating that the evapotranspiration is mainly composed of plant transpiration in the *Pinus yunnanensis* ecosystem. We also presented the temporal variation of LAI in the observing days, showing general similar trend with the average T/ET. However, the ratio becomes relatively constant after the *Pinus yunnanensis* established dense foliage (LAI > 5.24), confirming that T/ET ratio become less sensitive to LAI variation in the late growing season (Zhou et al., 2016).

We used the T/ET acquired from the two isotopes measurement, and eddy covariance measured ET, ranging from 0.8 to 2.2 mm $d^{-1}$ and with an average of 1.8 mm $d^{-1}$, to partition the seasonal variations of soil evaporation (E) and plant transpiration (T) only on clear days (Fig. 8). We identified a clear seasonal pattern of transpiration, increasing from about 0.47 mm $d^{-1}$ in the beginning of June, to over 1.0 mm $d^{-1}$ abruptly from the middle of June, and keeping higher value until to the end of observation. Soil evaporation, however, shows little variations throughout the observation period, varying in the range of 0.32 to 0.64 mm $d^{-1}$. Therefore, the seasonal variations of evapotranspiration are mainly due to the change in transpiration, less from soil evaporation.

## 4. Discussion

### 4.1. Comparison of T/ET ratio in a global scale

Partitioning ET is expected to become increasingly important as available water resources continue to diminish. An improved understanding of where losses occur and how much water is used through plant transpiration can benefit the understanding of the hydrologic systems which affect stream flow, ground water recharge and weather conditions, as well as plant biomass production and associated carbon sequestration (Kool et al., 2014). In this section we further compared our results of the estimated midday T/ET with previous studies (Fig. 9) in a broad space scale. This summary of the available estimated midday T/ET ratios on regional and global includes a diverse range of ecosystems, such as cropland, grassland, woodland, shrubland and paddy fields in Africa, Europe, America, Asia and Oceania. We see a large range of midday T/ET estimation of 0.15-0.98 owing to different approaches used in the estimation and different research scales and ecosystems. As a comparison, we also added our result in this graph. The range of midday T/ET (0.59-0.81) in our study, is within the broad range of previous studies (Schlesinger and Jasechko, 2014; Wang-Erlandsson et al., 2014; Zhou et al., 2016; Fatichi and Pappas, 2017). Our midday average T/ET (0.73 ± 0.06) value were slightly higher than results from global long-term average. One likely reason is that the estimated midday T/ET ratio is observed in the hours of maximum transpiration, but not a daily average. Another possible influence is the lack of observation for intercepted precipitation by vegetation canopy in our study, as isotope observations were only conducted during the clear periods. Evaporation

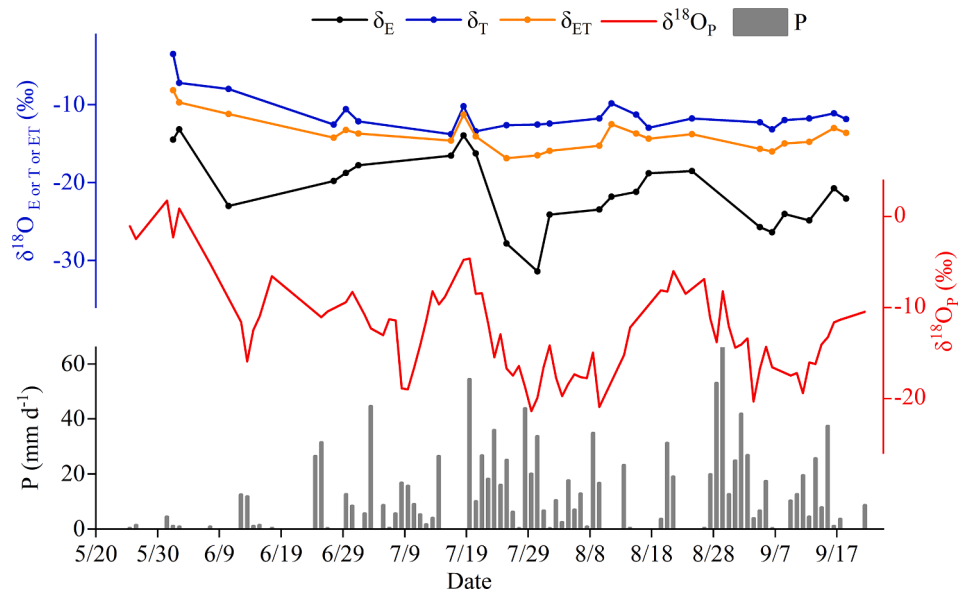


**Fig. 6.** Seasonal variations of daily precipitation $\delta^{18}O$ and $\delta_E$ (black circles), $\delta_T$ (blue circles) and $\delta_{ET}$ (orange circles) for $\delta^{18}O$ at early afternoon (13:00-15:00), and daily precipitation amount as a comparison.

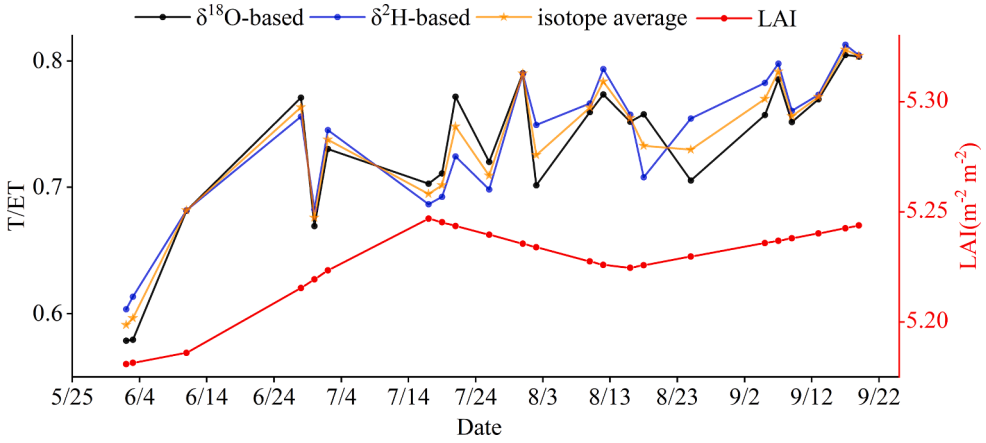


**Fig. 7.** Seasonal variations of $\delta^{18}O$-based (black circles) and $\delta^2H$-based T/ET (blue circles) and their average (orange circles) for midday periods (13:00-15:00). Leaf area index (LAI) (red circles) was also shown for reference.

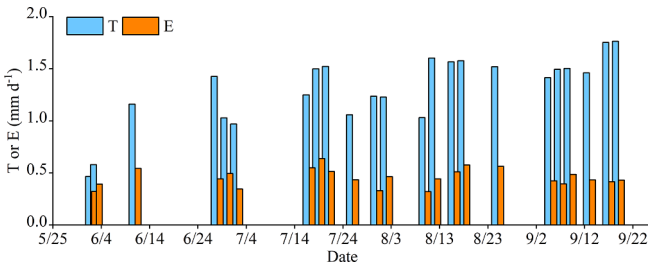


**Fig. 8.** Seasonal variations of T and E calculated from isotope-based T/ET and eddy covariance measured ET based on May to September of 2019 (only on clear days).

over vegetation canopy interception was not included in evapotranspiration for Keeling-CG methods. However, interception (dew or preceding rain) may even present in no-rain period and bias the values of $\delta_T$ and $\delta_{ET}$. Measurements conducted in this condition should be excluded and not involved in T/ET calculation. On raining days, interception evaporation may constitute a significant part of evapotranspiration (Miralles et al., 2010; Wei et al., 2017). Additionally, the evergreen coniferous forests are distributed in humid climates zone with higher wet canopy evaporation rates than other biomes, and therefore enhancing this effect (Wei et al., 2017). Hence, our estimated midday T/ET of 0.73 may be, to some extent, overestimated (when compared to long-term means) due to the lack of interception evaporation after precipitation. Different techniques and study scales may also lead to the variability, for instance hydrometric and isotope-based methods produce higher transpiration fraction values than the models driven by meteorological measurements and sap flow meters (Sutanto et al., 2014). Seasonal T/ET can be extremely variable within a given year at the same site in association with climate change and differential plant responses (Scott et al., 2006). In this study, the T/ET variation shows a strong seasonality, with the lowest value of 0.5-0.7 in pre-monsoon season of June, and higher ratio of approximately of 0.7-0.8 throughout the monsoon season. T/ET increased almost continuously with the vegetation growth in the early growing season, and became relatively constant after the *Pinus yunnanensis* established dense foliage (LAI > 5.24). T/ET ratios estimated from both $\delta^{18}O$ and $\delta^2H$ are quite consistent, but the estimate from $\delta^2H$ is slightly higher than from $\delta^{18}O$ in average, in particular, in the heavy raining days during August-

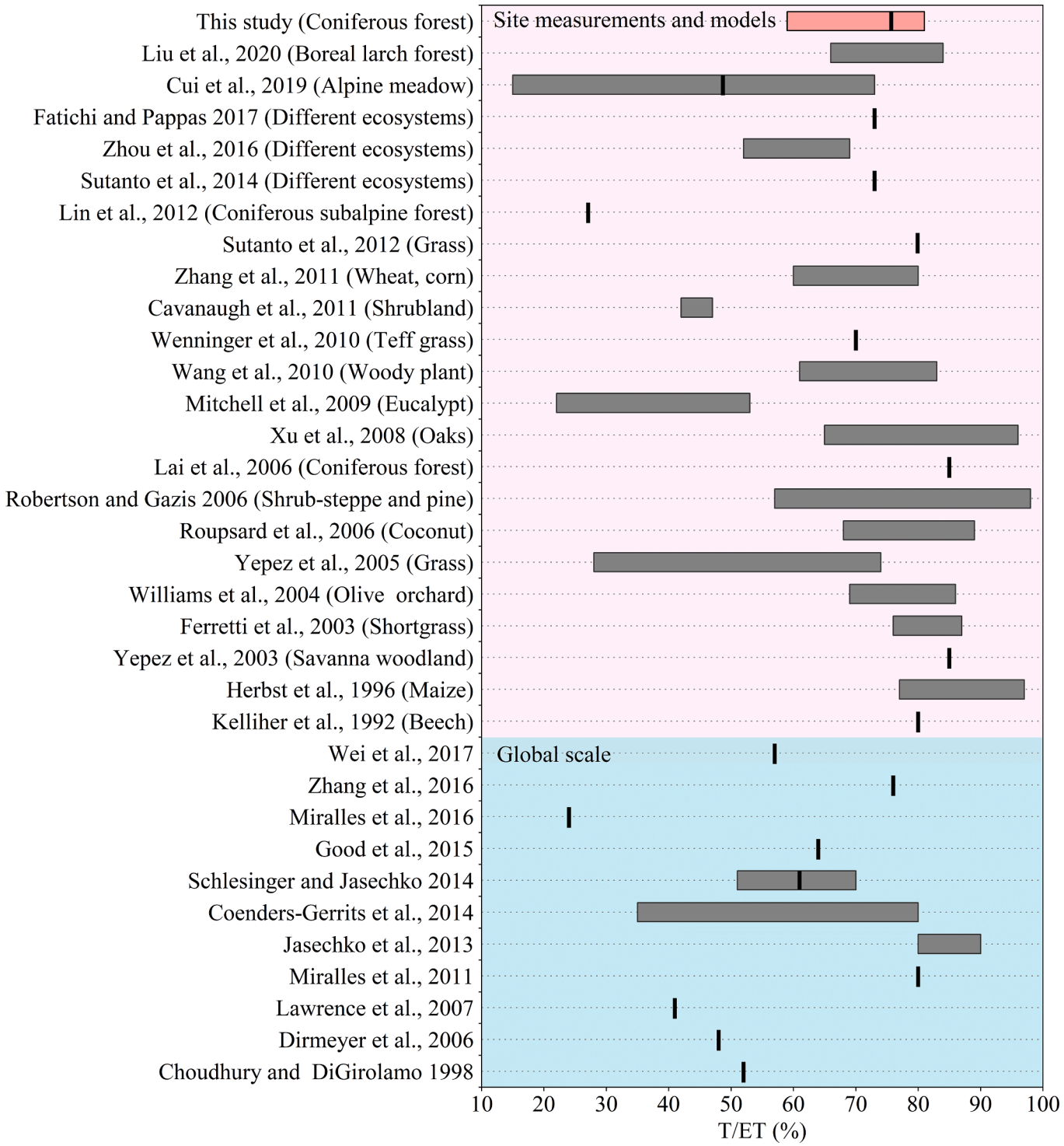


**Fig. 9.** Comparison of T/ET estimated by different methods from global and spot scale. Pink area is for spot measurements and models and blue area is for global scale results. The plot by vegetation or ecosystem type are indicated in brackets. The vertical line represents the reported average values and the rectangle represents the ranges of T/ET in the published literatures.

September. Overall, transpiration is the most robust engine for water transportation in southwest forest, consistent with other ecosystems worldwide (Schlesinger and Jasechko, 2014).

### 4.2. *Factors influencing T/ET estimation in the forest ecosystem*

To evaluate how environmental (Swc, VPD and Ta) and biological factors (here we considered only LAI) influencing the seasonal T/ET variations, correlation analysis and partial correlation analysis were performed between these daily values with T/ET ratios (Fig. 10). The correlation analysis results show that Swc and LAI have a significant influence on T/ET and are the primary controlling factor, followed by Ta and VPD.

Previous studies have consistently demonstrated that there is an observable relationship between T/ET and LAI at the seasonal scale (Wang et al., 2014; Wei et al., 2015; Berkelhammer et al., 2016). Our

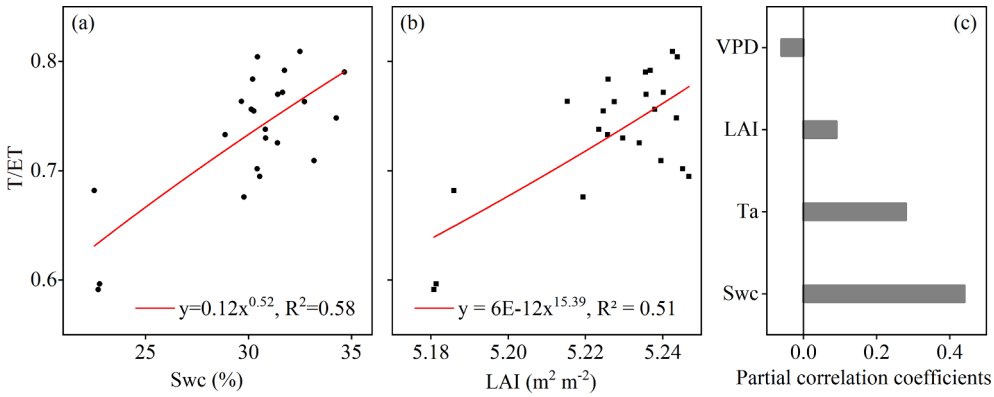


**Fig. 10.** Relationships between daily isotope-based T/ET and daily average of volumetric soil water content (Swc) at 5, 20, 40 cm depth (a) and LAI (b) and partial correlation coefficients between T/ET and Swc, LAI, vapor pressure deficit (VPD) and Ta (c) at Lijiang station.

isotope-based results reconfirmed this relationship, verifying that LAI plays an important role in the hydrological cycle of alpine coniferous ecosystems at entire raining season. Critically, we found the influence of Swc is of sufficient magnitude comparable to the impact of LAI on the seasonal T/ET variation (Fig. 10a-b). Partial correlation analysis further suggests that the individual contribution from Swc is more substantial than that of LAI (Fig. 10c). This may be because that the T/ET for evergreen vegetation is mainly controlled by soil water content, since the inter-annual change in vegetation cover is quite small for evergreens (Zhou et al., 2016). In addition, LAI varies little in alpine forest regions at entire raining season. The larger LAI (representing tree size and density) will enhance transpiration while curb evaporation, both because of the larger tree canopy and because of the larger shaded under-canopy fraction (Raz-Yaseef et al., 2012).

Based on the observations on the forest ecosystem in SW China, we have developed an explanation of the underlying mechanisms controlling the changes of T/ET at seasonal scales. The lower T/ET in spring was related to the lower LAI in the early stage of the growing season, combined with lower Swc corresponding to less precipitation. LAI reached a peak in summer, and intense precipitation elevated Swc, and thus brought sufficient water for high levels of plant transpiration. Under the same LAI condition, increasing soil moisture may reduce T/ET via increasing soil E (Wei et al., 2018). Other authors have also emphasized the role of soil water content in controlling T/ET (Hu et al. 2009; Liu et al., 2002). Although T/ET was well correlated with Swc at the forest ecosystem in SW China (Fig. 10a), the relationship may have regional variation and not be ubiquitous, instead being vegetation type-related or spatiotemporal scales-related. According to a global T/ET dataset, as synthesized by Wang et al. (2014) showed generally low correlations with soil water potential. However, Swc was a constraining factor in arid or semi-arid climates, but not in humid or semi-humid climates. Limited studies that have reported the Swc dependence to date were located in croplands (e.g., Liu et al., 2002; Wei et al., 2018). Taking the example of wheat, the main depths of root water uptake are from 0 to 40 cm depths, while soil evaporation is controlled by soil moisture at the depth<20 cm (Zhang et al., 2011), again causing weak correlations between T/ET and Swc. Hence, we are cautious to believe that both environmental (partial correlation coefficient: 0.44) and biological factors (0.09) dominated the variations of T/ET in our alpine coniferous ecosystem region in southwest China, but only in June-September, against with the previous studies that arguing T/ET is mainly controlled by LAI (Hu et al., 2009; Wei et al., 2015). The same results also found in other ecosystems of earlier studies (Cui et al., 2020; Liu et al., 2002). Actually, the correlation relationship analyzed in this study mainly reflects the influence of seasonal changes (Fig. 10). However, when focusing on a certain season (after June 28th), the relationship both LAI and Swc are not significant with T/ET ratios (Fig. A4). The specific influencing factors in a certain season need to be further studied. We are aware that this conclusion is very limited, as our field experiments are from June to September, not cover a full year. A longer timeframe might demonstrate T/ET to have slightly different LAI and Swc dependencies at alpine forest regions. Future measurement campaigns that cover a full year, will enable testing of our discovered relationships between T/ET, LAI and Swc during other seasons.

### 4.3. *Performance of chamber method in the forest ecosystem*

To evaluate the performance of each method in estimating $\delta_E$ and $\delta_T$, estimated isotopic composition from different methods (new customized chamber and Craig-Gordon model) are presented for comparison (Fig. 11). The time series diagrams of $\delta_E$ and $\delta_T$ estimated by the two methods are also presented to discern the detail differences between the two methods (Fig. A5). The new customized chamber method presented in this study shows good agreements with Craig-Gordon model. the results from the chamber-based mass balance approach and the Craig-Gordon model matches well in $\delta_E$, with $R^2$ of 0.82, 0.88 ($P < 0.01$), respectively for $\delta^{18}O$ and $\delta^2H$ (Fig. 11). For $\delta_T$, the relation coefficients are $R^2$ of 0.63, 0.65 ($P < 0.01$), respectively for $\delta^{18}O$ and $\delta^2H$. These statistics are encouraging and highlights the robustness of the chamber method in evaluation for evaporation E and transpiration T. The $\delta_E$ values of C-G model calculation is slightly lower than the chamber-based method ($-21.0 \pm 4.5$‰ vs. $-18.6 \pm 3.8$‰ for C-G model calculations and chamber-based for $\delta^{18}O$, respectively). The enrichment result (~2‰) is most likely caused by air condensation inside the chamber or sampling tube. This is generally consistent with the suggestion of that the $\delta_E$ values for $\delta^2H$ of chamber method were consistently more enriched than the C-G model calculations (Wang et al, 2013). This may be because of an inherent limitation of the chamber method in association with its impact on environmental conditions inside the chamber, potentially affecting the measured isotope values (Dubbert et al., 2014). Air temperature in the chamber increased ~ 2 °C above ambient levels after 5 min in an open cork-oak woodland (Dubbert et al., 2014). This warming inadvertently enhanced the estimated soil evaporation in the chamber, enriched $\delta_E$ relative to the C-G model (Wang et al., 2013). Another possible reason for the enrichment result (~2‰) between C-G model calculations and chamber method is that the uncertainties of kinetic enrichment factor ($\varepsilon_k$) in C-G model, which εk associated with diffusion of water through the soil (Zhang et al., 2010). Additionally, this may also lead to systematic bias because of the identification of the evaporating front in C-G model (Dubbert et al., 2013). The location of evaporation fronts is influenced by meteorological conditions, soil water content and soil texture (Zimmermann et al., 1967). Using the C-G model in conjunction with a climate chamber-controlled experiment, Rothfuss et al. (2010) showed that the failure to determine the evaporating front may produce a large bias within. These consistence in the C-G model calculations and chamber-based observation confirmed the

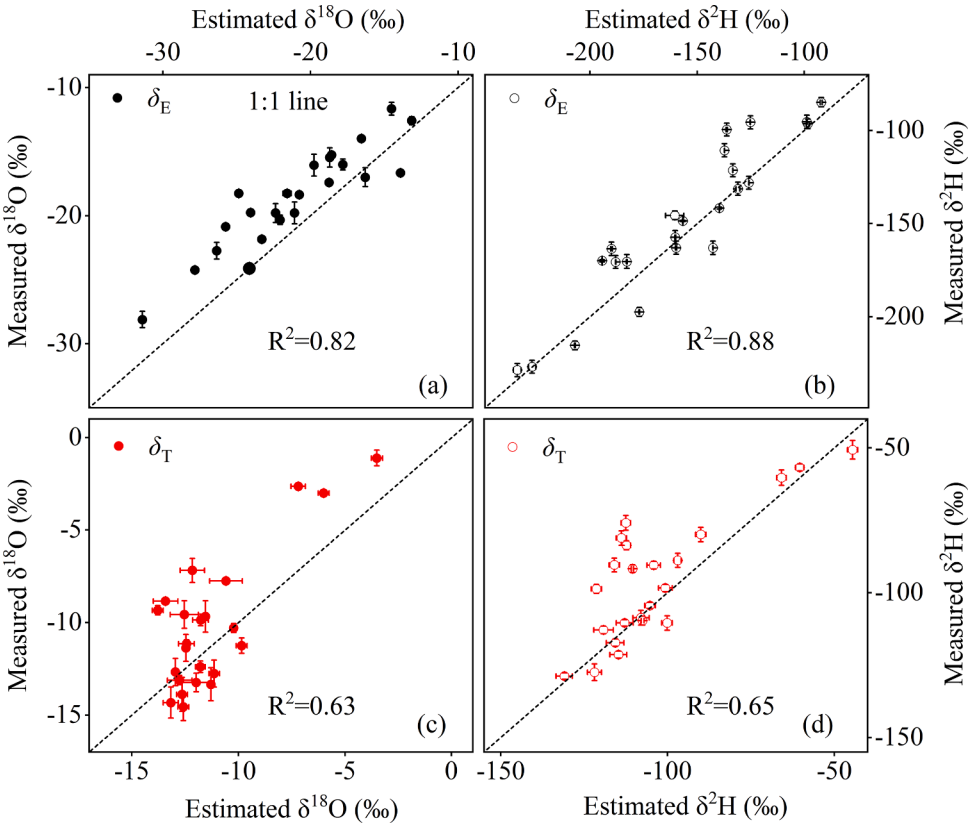


**Fig. 11.** Scatter plot of the modeled $\delta_E$ and $\delta_T$ against the measured $\delta_E$ and $\delta_T$ of $\delta^{18}O$ and $\delta^2H$ during experimental period. Upper panel shows the squared correlation coefficients between the modeled $\delta_E$ and the measured $\delta_E$ respectively for $\delta^{18}O$ (black circles) (a) and $\delta^2H$ (open black circles) (b) was 0.82, 0.88. ($P < 0.01$), respectively. Bottom panel shows the squared correlation coefficients between the modeled $\delta_T$ and the observed $\delta_T$ respectively for $\delta^{18}O$ (red circles) (c) and $\delta^2H$ (open red circles) (d) was 0.63, 0.65. ($P < 0.01$), respectively. Error bars depict the standard deviation for $\delta_T$ and $\delta_E$ in each measurement.

representative of vegetation in the chamber, although we also suggest the necessity of comparison in more extensive area.

The uncertainty in the measured isotope data from the chamber method is rather small. The average standard deviation of measured $\delta^{18}O$ and $\delta^2H$ of $\delta_T$ are 0.6 ‰ and 1.4 ‰ during the observations period, very close to the precision of laboratory-based values and lower than reported by Wang et al. (2012) (1.0 ‰ for $\delta^{18}O$ and 1.6 ‰ for $\delta^2H$). There was no significant difference of standard deviation between $\delta_E$ and $\delta_T$.

New customized chamber method will provide a new opportunity to investigate large-scale T or E behaviors, but require further validation for the independent measurements. The potential advantage of using the new customized chamber method is the relatively consistent error sources in the isotope compositions of three fluxes (e.g., from the same laser instrument), which might be diminished or even canceled out when calculating the ET partitioning (Wang et al., 2013).

### 4.4. *Uncertainty and possible error source in T/ET ratio estimation*

Here we made the sensitivity test results and discussed the uncertainties and possible error sources in the Keeling-CG method ($\delta_E$, $\delta_T$ and $\delta_{ET}$). The estimated $\delta_{ET}$ in this study was acquired by using the Keeling plot method. However, this method can produce uncertainty and errors which is inherent in the Keeling plots (Pataki et al., 2003; Nickerson and Risk, 2009; Wei et al., 2015). Earlier studies showed that the error in $\delta_{ET}$ estimation could be quite large even for a high $R^2$ value in the Keeling plots (e.g., atmospheric fluctuations and unsteady diffusion) (Lee et al., 2006; Nickerson and Risk, 2009). Therefore, to constrain the uncertainty in the estimated T/ET ratio, we made the sensitivity test by assuming a ±1σ variation in $\delta_{ET}$. The results showed a ±1σ changes in $\delta_{ET}$, will result in a T/ET ratio change of 0.30% ~ 0.28% from $\delta_{ET}{}^{18}O$, and 0.50% ~ -0.50% from $\delta_{ET}{}^2H$ (Table 1). The total uncertainties in average ±1σ is -13.8 ±2.1‰ for $\delta_{ET}{}^{18}O$ and -117.0 ± 20.2‰ for $\delta_{ET}{}^2H$. However, we argue that the bias from $\delta_{ET}$ could be small, since we did not find large variability of $\delta_{ET}$ observed in the midday (13:00-15:00) (Fig. 6).

**Table 1**
Sensitivity test results of $\delta_E$ $\delta_T$ or $\delta_{ET}$ variation on T/ET ratio (in %) with a ± 1σ variation in the Keeling-CG method.

| The bias in T/ET ratio | $\delta^{18}O$ | | $\delta^2H$ | |
|---|---|---|---|---|
| | +1σ | −1σ | +1σ | −1σ |
| Based on $\delta_E$ variation | −0.30 | 0.12 | −0.89 | 0.16 |
| Based on $\delta_T$ variation | −0.19 | 0.34 | −0.27 | 0.65 |
| Based on $\delta_{ET}$ variation | 0.30 | −0.28 | 0.50 | −0.50 |

Then we evaluated the uncertainty derived from $\delta_E$ variations. The water $\delta^{18}O$ at the soil evaporating front $\delta_S$ mainly controls the estimation of $\delta_E$ in the model (Craig and Gordon, 1965). Therefore, precise determination of the evaporating front depth was critical because $\delta_S$ varied considerably near the evaporating front (Dubbert et al., 2013). In this study, the vertical variations of soil water $\delta^{18}O$ indicate that the evaporating front is at 5 cm. The use of evaporating front water in other soil depth would induce a maximum T/ET bias of 0.16% and 0.34%, based on $\delta^{18}O$ and $\delta^2H$, respectively. In the sensitivity test, we also showed that a ± 1σ changes in $\delta_E$, will result in a T/ET ration change of −0.30% to 0.12% from $\delta_E{}^{18}O$, and −0.89% to 0.16% from $\delta_E{}^2H$ (Table 1). The test result shows that the estimated T/ET ratio change could be large, in particular with $\delta_E{}^2H$ decrease. The total uncertainties in average ± 1σ is −21.0 ± 4.6‰ for $\delta_E{}^{18}O$ and −156.4 ± 39.0‰ for $\delta_E{}^2H$.

In terms of the variations of $\delta_T$, the bias in the simulated T/ET ratio could be −0.19% ~ 0.34% from $\delta_T{}^{18}O$, and −0.27% ~ 0.65% from $\delta_T{}^2H$ (Table 1), with a ± 1σ changes in $\delta_T$. The total uncertainties in average ± 1σ is −11.2 ± 2.5‰ for $\delta_T{}^{18}O$ and −103.7 ± 20.8‰ for $\delta_T{}^2H$. This uncertainly is mainly resulted from the short observation hours while a full day observation is unavailable. Fortunately, although a full day

observation is encouraged (Williams et al., 2004), short hours observation in midday and early afternoon is more in practice (Sutanto et al., 2014). This is because the isotopic steady state (ISS) is achieved by midday and/or early afternoon, and transpiration from plants is usually at its maximum with a short turnover time of leaf water, and thus constrains $\delta_T$ close to the isotopic composition of plant source water (Wen et al., 2016). Additionally, although some studies mentioned NSS occurs even in midday for forests (e.g., Lai and Ehleringer, 2011), our results show that $\delta_{ET}$ fall in the range bounded by $\delta_T$ and $\delta_E$, such that $\delta_E < \delta_{ET} < \delta_T$, indicating that isotopic steady state (ISS) was reached during the midday (13:00–15:00). Therefore, we suggested that an ISS was a reasonable assumption in our observations.

## 5. Conclusions

We presented a detailed observation work on the seasonal variation of dual isotopes in various water reservoirs and the isotope signal transfers in between, including atmospheric vapor, precipitation, soil water and xylem water in an alpine forest ecosystem during the growing season in southwest China. The seasonal isotope signals in various water reservoirs tell a detailed transfer processes from precipitation to soil water, xylem water and leaf water with the involved fractionation, allowing for a diagnose of the evapotranspiration for the specific *Pinus yunnanensis* ecosystem. We made an estimation of the T/ET ratio by using the isotope approach. The estimated seasonal T/ET ranged from 0.59 to 0.81, with a near continuous increase over time in the early growing season and a plateau level of over 0.75 during the peak growing season. The mean T/ET ratio of 0.73 ± 0.06, is within the broad range of previous literature but slightly higher than global long-term average, highlights the importance of transpiration in the total evapotranspiration in the *Pinus yunnanensis* ecosystem. We also identified a clear seasonal pattern of transpiration, increasing from about 0.47 mm $d^{-1}$ in the beginning of June, to over 1.0 mm $d^{-1}$ abruptly from the middle of June, and keeping higher value until to September. A simple driver analysis showed that T/ET was correlated with environmental conditions (here, soil water content, Swc) in alpine forest regions at entire raining season (in June-September), in addition to LAI, challenging the earlier recognition of LAI dominated control. This result is likely related to the slight changes of LAI in the growing season for *Pinus yunnanensis* ecosystem. Hence, longer time continuous monitoring is still necessary, and we are also aware the sensitivity of controls on estimated T/ET at different time scale interested.

Comparison of the results of customized chamber and Craig-Gordon model demonstrated that the two methods are in robust consistence in estimating $\delta_E$ or $\delta_T$, with high correlation coefficients. Our results here highlighted the reliability of chamber method in isotope water cycle in the ecosystem with reasonable uncertainty, and reconfirm the findings to observe $\delta_{ET}$ by using the chamber method directly, and comparing it with other methods, such as Keeling plot approach, sap-flow meters, Bowen ratio systems, lysimeters and eddy covariance systems, as well as methods to isolate the individual T and E components.

These results presented in this paper shed light on the mechanisms underlying temporal change of terrestrial transpiration, and will provide far reaching impact on alpine forest managers and ecosystem protection under ongoing climate change.

## CRediT authorship contribution statement

**Jiaojiao Han:** Methodology, Investigation, Writing – original draft. **Lide Tian:** Conceptualization, Supervision, Writing – review & editing. **Zhongyin Cai:** Methodology, Writing – review & editing. **Wei Ren:** Methodology, Writing – review & editing. **Weiwei Liu:** Investigation, Resources. **Jin Li:** Investigation, Resources. **Jiangrong Tai:** Investigation, Data curation.

## Declaration of Competing Interest

The authors declare that they have no known competing financial interests or personal relationships that could have appeared to influence the work reported in this paper.

## Acknowledgements

We thank two reviewers and editor for their valuable comments and suggestions. This work was supported by the Strategic Priority Research Program of Chinese Academy of Sciences (Grant No. XDB40000000); the National Natural Science Foundation of China (Grant No. 41771043) and the Applied Basic Research Foundation of Yunnan Province (Grant No. 202001BB050066). We thank staff in Yunnan Lijiang Forest Ecosystem National Observation and Research Station, Kunming Institute of Botany, Chinese Academy of Sciences for their assistance.

## Appendix A. Supplementary data

Supplementary data to this article can be found online at https://doi.org/10.1016/j.jhydrol.2022.127672.

## References

Altieri, V., De Franco, S., Lombardi, F., Marziliano, P.A., Menguzzato, G., Porto, P., 2018. The role of silvicultural systems and forest types in preventing soil erosion processes in mountain forests: a methodological approach using cesium-137 measurements. J. Soils Sediments 18 (12), 3378–3387. https://doi.org/10.1007/s11368-018-1957-8.

Aguiar, M.R., Paruelo, J.M., Sala, O.E., Lauenroth, W.K., 1996. Ecosystem responses to changes in plant functional type composition: an example from the Patagonian steppe. J. Vegetat. Sci. 7 (3), 381–390. https://doi.org/10.2307/3236281.

Berkelhammer, M., Noone, D.C., Wong, T.E., Burns, S.P., Knowles, J.F., Kaushik, A., Blanken, P.D., Williams, M.W., 2016. Convergent approaches to determine an ecosystem's transpiration fraction. Global Biogeochem. Cycles 30 (6), 933–951.

Coenders-Gerrits, A.M.J., van der Ent, R.J., Bogaard, T.A., Wang-Erlandsson, L., Hrachowitz, M., Savenije, H.H.G., 2014. Uncertainties in transpiration estimates. Nature 506 (7487), E1–E2. https://doi.org/10.1038/nature12925.

Craig, H., 1961. Isotopic variations in meteoric waters. Science 133 (3465), 1702–1703. https://doi.org/10.1126/science.133.3465.1702.

Craig, H., Gordon, L.I., 1965. In: Deuterium and oxygen-18 variations in the ocean and the marine atmosphere. Lischi and Figli, Pisa, pp. 9–130.

Cui, J.B., Tian, L.D., Gerlein-Safdi, C., Qu, D.M., 2017. The influence of memory, sample size effects, and filter paper material on online laser-based plant and soil water isotope measurements. Rapid Commun. Mass Spectrom. 31 (6), 509–522. https://doi.org/10.1002/rcm. 7824.

Cui, J.B., Tian, L.D., Wei, Z.W., Huntingford, C., Wang, P., Cai, Z.Y., Ma, N., Wang, L.X., 2020. Quantifying the controls on evapotranspiration partitioning in the highest alpine meadow ecosystems. Water Resour. Res. 56 (4) https://doi.org/10.1029/2019WR024815.

Dawson, T.E., Ehleringer, J.R., 1993. Isotopic enrichment of water in the woody tissues of plant: implications for plant water source, water uptake, and other studies which use stable isotopes. Geochimica et Casmachimica Acta. 57(14), 3487-3492. https://doi.org/ 7037(93)90554-A.

Dubbert, M., Cuntz, M., Piayda, A., Maguás, C., Werner, C., 2013. Partitioning evapotranspiration–Testing the Craig and Gordon model with field measurements of oxygen isotope ratios of evaporative fluxes. J. Hydrol. 496, 142–153. https://doi.org/10.1016/j.jhydrol.2013.05.033.

Dubbert, M., Cuntz, M., Piayda, A., Werner, C., 2014. Oxygen isotope signatures of transpired water vapor: the role of isotopic non-steady-state transpiration under natural conditions. New Phytol. 203 (4), 1242–1252. https://doi.org/10.3389/fpls.2014.00530.

Eichelmann, E., Hemes, K.S., Knox, S.H., Oikawa, P.Y., Chamberlain, S.D., Sturtevant, C., Verfaillie, J., Baldocchi, D.D., 2018. The effect of land cover type and structure on evapotranspiration from agricultural and wetland sites in the Sacramento- San Joaquin River Delta. California. Agric. For. Meteorol. 256–257, 179–195. https://doi.org/10.1016/j.agrfo rmet.2018.03.007.

Fatichi, S., Pappas, C., 2017. Constrained variability of modeled T: ET ratio across biomes : Transpiration:Evapotranspiration Ratio. Geophys. Res. Lett. 44 (13), 6795–6803.

Feng, J.M., Wang, X.P., Xu, C.D., Yang, Y.H., Fang, J.Y., 2006. Altitudinal patterns of plant species diversity and community structure on Yulong Mountains, Yunnan. China. J. Mt. Sci. 24 (1), 110–116.

Good, S.P., Noone, D., Bowen, G., 2015. Hydrologic connectivity constrains partitioning of global terrestrial water fluxes. Science 349 (6244), 175–177. https://doi.org/10.1126/science.aaa5931.

Good, S.P., Soderberg, K., Guan, K., King, E.G., Scanlon, T.M., Caylor, K.K., 2014. $\delta^2H$ isotopic flux partitioning of evapotranspiration over a grass field following a water

pulse and subsequent dry down. Water Resour. Res. 50 (2), 1410–1432. https://doi.org/10.1002/2013WR014333.
Hansen, M.C., Potapov, P., Margono, B., Stehman, S., Turubanova, S., Tyukavina, A., 2014. Response to Comment on "High-resolution global maps of 21st-century forest cover change. Science 344 (6187), 981. https://doi.org/10.1126/science.1248817.
He, Y.Q., Yao, T.D., Theakstone, W.H., Cheng, G.D., Yang, M.X., Chen, T., 2002. Recent climatic significance of chemical signals in a shallow firn core from an alpine glacier in the South-Asia monsoon region. J. Asian Earth Sci. 20 (3) https://doi.org/10.1016/s1367-9120(01)00038-4.
Hu, Z.M., Yu, G.R., Zhou, Y.L., Sun, X.M., Li, Y.N., Shi, P.L., Wang, Y.F., Song, X., Zheng, Z.M., Zhang, L., Li, S.G., 2009. Partitioning of evapotranspiration and its controls in four grassland ecosystems: application of a two-source model. Agric. For. Meteorol. 149 (9), 1410–1420. https://doi.org/10.1016/j.agrformet.2009.03.014.
Jasechko, S., Sharp, Z.D., Gibson, J. J., Birks, S. J., Yi, Y., Fawcett, P. J., 2013. Terrestrial water fluxes dominated by transpiration. Nature. 496(7445), 347-350. https://doi.org/10. 1038/nature11983.
Jefferson, J.L., Maxwell, R.M., Constantine, P.G., 2017. Exploring the sensitivity of photosynthesis and stomatal resistance parameters in a Land Surface Model. J. Hydrometeorol. 18 (3), 897–915. https://doi.org/10.1175/JHM-D-16-0053.1.
Jung, M., Reichstein, M., Ciais, P., Seneviratne, S.I., Sheffield, J., Goulden, M.L., Bonan, G., Cescatti, A., Chen, J., de Jeu, R., Dolman, A.J., Eugster, W., Gerten, D., Gianelle, D., Gobron, N., Heinke, J., Kimball, J., Law, B.E., Montagnani, L., Mu, Q., Mueller, B., Oleson, K., Papale, D., Richardson, A.D., Roupsard, O., Running, S., Tomelleri, E., Viovy, N., Weber, U., Williams, C., Wood, E., Zaehle, S., Zhang, K.e., 2010. Recent decline in the global land evapotranspiration trend due to limited moisture supply. Nature 467 (7318), 951–954.
Keeling, C.D., 1958. The concentration and isotopic abundances of atmospheric carbon dioxide in rural areas. Geochim. Geochim. Cosmochim. Acta 13 (4), 322–334. https://doi.org/10.1016/0016-7037(58)90033-4.
Kochendorfer, J.P., Ramírez, J.A., 2010. Ecohydrologic controls on vegetation density and evapotranspiration partitioning across the climatic gradients of the central United States. Hydrol. Earth Syst. Sci. Discuss. 14 (10), 2121–2139. https://doi.org/10.5194/hess-14-2121-2010.
Kool, D., Agam, N., Lazarovitch, N., Heitman, J.L., Sauer, T.J., Ben-Gal, A., 2014. A review of approaches for evapotranspiration partitioning. Agric. For. Meteorol. 184, 56–70. https://doi.org/10.1016/j.agrformet.2013.09.003.
Lai, C.T., Ehleringer, J.R., 2011. Deuterium excess reveals diurnal sources of water vapor in forest air. Oecologia. 165 (1), 213–223. https://doi.org/10.1007/s00442-010-1721-2.
Lawrence, D.M., Thornton, P.E., Oleson, K.W., Bonan, G.B., 2007. The partitioning of evapotranspiration into transpiration, soil evaporation, and canopy evaporation in a GCM: impacts on land–atmosphere interaction. J. Hydrometeorol. 8(4), 862–880. https://doi.org/ 10.1175/JHM596.1.
Lee, X.H., Smith, R., Williams, J., 2006. Water vapor $^{18}o/^{16}o$ isotope ratio in surface air in New England, USA. Tellus Ser. B. 58 (4), 293–304. https://doi.org/10.1111/j.1600-0889.2006.00191.x.
Lian, X., Piao, S.L., Huntingford, C., Li, Y., Zeng, Z.Z., Wang, X.H., Ciais, P., McVicar, T. R., Peng, S.S., Ottlé, C., Yang, H., Yang, Y.T., Zhang, Y.Q., Wang, T., 2018. Partitioning global land evapotranspiration using CMIP5 models constrained by observations. Nat. Clim. Change. 8 (7), 640–646. https://doi.org/10.1038/s41558-018-0207-9.
Lin, Y.X., Zhang, Y.P., Fei, X.H., Song, Q.H., Xu, K., Deng, Y., Liu, W.W., Chen, A. G., Li, P.G., Huang, H., Jin, Y.Q., Li, J., 2019. Comparative study of evapotranspiration characteristics over different forest ecosystems in Yunnan Province, Southwest China. Journal of Yunnan University: Natural Sciences Edition. 41(1), 205-218. https://doi.org/ 10.7540/j.ynu.20170568.
Liu, C.M., Zhang, X.Y., Zhang, Y.Q., 2002. Determination of daily evaporation and evapotranspiration of winter wheat and maize by large-scale weighing lysimeter and microlysimeter. Agric. For. Meteorol. 111 (2), 109–120. https://doi.org/10.1016/s0168-1923(02)00015-1.
Liu, X.M., Zhang, D., 2012. Trend analysis of reference evapotranspiration in northwest China: the roles of changing wind speed and surface air temperature. Hydrol. Process. 27 (26), 3941–3948. https://doi.org/10.1002/hyp.9527.
Liu, J.L., Cheng, F.Y., Munger, W., Jiang, P., Whitby, T.G., Chen, S.Y., Ji, W.W., Man, X. L., 2020. Precipitation extremes influence patterns and partitioning of evapotranspiration and transpiration in a deciduous boreal larch forest. Agric. For. Meteorol. 287, 107936. https://doi.org/10.1016/j.agrformet.2020.107936.
Lu, X., Liang, L.L., Wang, L., Jenerette, G.D., McCabe, M.F., Grantz, D.A., 2017. Partitioning of evapotranspiration using a stable isotope technique in an arid and high temperature agricultural production system. Agric. Water Manage. 179 (C), 103–109. https://doi.org/10.1016/j.agwat.2016.08.012.
Luo, Y.H., Liu, J., Tan, S.L., Cadotte, M.W., Wang, Y.H., Xu, K., Li, D.Z., Gao, L.M., Reinhart, K.O., 2016. Trait-Based community assembly along an elevational gradient in subalpine forests: quantifying the roles of environmental factors in inter- and intraspecific variability. PLoS One 11 (5), e0155749-. https://doi.org/10.1371/journal.pone.0155749.
Ma, N., Niu, G.-Y., Xia, Y., Cai, X., Zhang, Y., Ma, Y., Fang, Y., 2017. A systematic evaluation of noah-MP in simulating land-atmosphere energy, water, and carbon exchanges over the continental United States. J. Geophys. Res. Atmos. 122 (22), 12,245–12,268.
Majoube, M., 1971. Fractionnement en oxygene-18 et en deuterium entre lfeau et sa vapeur. J. Chim. Phys. 68, 1423–1436. https://doi.org/10.1051/jcp/1971681423.
Maxwell, R.M., Condon, L.E., 2016. Connections between groundwater flow and transpiration partitioning. Science 353 (6297), 377–380. https://doi.org/10.1126/science.aaf7891.
Merlivat, L., 1978. Molecular diffusivities of $H_2{}^{16}O$, $HD^{16}O$ and $H_2{}^{18}O$ in gases. J. Chem. Phys. 69 (6), 2864–2871. https://doi.org/10.1063/1.436884.
Miralles, D.G., Gash, J.H., Holmes, T.R.H., de Jeu, R.A.M., Dolman, A.J., 2010. Global canopy interception from satellite observations. J. Geophys. Res. 115 (D16), D16122. https://doi.org/10.1029/2009jd013530.
Miralles, D.G., Jiménez, C., Jung, M., Michel, D., Ershadi, A., McCabe, M.F., Hirschi, M., Martens, B., Dolman, A.J., Fisher, J.B., Mu, Q., Seneviratne, S.I., Wood, E.F., Fernández-Prieto, D., 2016. The WACMOS-ET project-Part 2: evaluation of global terrestrial evaporation data sets. Hydrol. Earth Syst. Sci. 20 (2), 823–842. https://doi.org/10.5194/hess-20-823-2016.
Newman, B.D., Wilcox, B.P., Archer, S.R., Breshears, D.D., Dahm, C.N., Duffy, C.J., McDowell, N.G., Phillips, F.M., Scanlon, B.R., Vivoni, E.R., 2006. Ecohydrology of water-limited environments: A scientific vision. Water Resour. Res. 42(6), n/a–n/a. doi:10.1029/2005wr004141.
Nickerson, N., Risk, D., 2009. Keeling plots are non-linear in non-steady state diffusive environments. Geophys. Res. Lett. 36 (8) https://doi.org/10.1029/2008gl036945.
Niu, H.W., He, Y.Q., Zhu, G.F., Xin, H.J., Du, J.K., Lu, X.X., Pu, T., Zhao, G.Y., 2013. Environmental implications of the snow chemistry from Mt Yulong, southeastern Tibetan Plateau. Quatern Int. 313–314, 168–178. https://doi.org/10.1016/j.quaint.2012.11.019.
Pataki, D.E., Ehleringer, J.R., Flanagan, L.B., Yakir, D., Bowling, D.R., Still, C.J., Buchmann, N., Kaplan, J.O., Berry, J.A., 2003. The application and interpretation of Keeling plots in terrestrial carbon cycle research. Global Biogeochem. Cy. 17 (1) https://doi.org/10.1029/2001gb001850.
Prince, S.D., Brown de Colstoun, E., Kravitz, L.L., 1998. Evidence from rain-use efficiencies does not indicate extensive Sahelian desertification. Global Change Biol. 4 (4), 359–374. https://doi.org/10.1046/j.1365-2486.1998.00158.x.
Quade, M., Klosterhalfen, A., Graf, A., Brüggemann, N., Hermes, N., Vereecken, H., Rothfuss, Y., 2019. In-situ monitoring of soil water isotopic composition for partitioning of evapotranspiration during one growing season of sugar beet (Beta vulgaris). Agric. For. Meteorol. 266–267, 53–64. https://doi.org/10.1016/j.agrformet.2018.12.002.
Raz-Yaseef, N., Yakir, D., Schiller, G., Cohen, S., 2012. Dynamics of evapotranspiration partitioning in a semi-arid forest as affected by temporal rainfall patterns. Agric. For. Meteorol. 157, 77–85. https://doi.org/10.1016/j.agrformet.2012.01.015.
Rigden, A.J., Salvucci, G.D., Entekhabi, D., Short Gianotti, D.J., 2018. Partitioning evapotranspiration over the continental United States using weather station data. Geophys. Res. Lett. 45 (18), 9605–9613. https://doi.org/10.1029/2018gl079121.
Rothfuss, Y., Biron, P., Braud, I., Canale, L., Durand, J.L., Gaudet, J.P., Richard, P., Vauclin, M., Bariac, T., 2010. Partitioning evapotranspiration fluxes into soil evaporation and plant transpiration using water stable isotopes under controlled conditions. Hydrol. Process. 24 (22), 3177–3194. https://doi.org/10.1002/hyp.7743.
Rozanski, K., Arguas-Arguas, L., Gongiantini, R., 1993. Isotope patterns in modern global precipitation, Geophysical Monograph 78, Climate Change in Continental Isotope Records. American Geophysical Union., pp. 1-36.
Schlesinger, W.H., Jasechko, S., 2014. Transpiration in the global water cycle. Agric. For. Meteorol. 189–190, 115–117. https://doi.org/10.1016/j.agrformet.2014.01.011.
Scott, R.L., Huxman, T.E., Cable, W.L., Emmerich, W.E., 2006. Partitioning of evapotranspiration and its relation to carbon dioxide exchange in a Chihuahuan Desert shrubland. Hydrol. Process. 20 (15), 3227–3243. https://doi.org/10.1002/hyp.6329.
Scott, R.L., Biederman, J.A., 2017. Partitioning evapotranspiration using long-term carbon dioxide and water vapor fluxes. Geophys. Res. Lett. 44 (13), 6833–6840. https://doi.org/10.1002/2017GL074324.
Steen-Larsen, H.C., Johnsen, S.J., Masson-Delmotte, V., Stenni, B., Risi, C., Sodemann, H., Balslev-Clausen, D., Blunier, T., Dahl-Jensen, D., Ellehøj, M.D., Falourd, S., Grindsted, A., Gkinis, V., Jouzel, J., Popp, T., Sheldon, S., Simonsen, S. B., Sjolte, J., Steffensen, J.P., Sperlich, P., Sveinbjörnsdóttir, A.E., Vinther, B.M., White, J.W.C., 2013. Continuous monitoring of summer surface water vapor isotopic composition above the Greenland Ice Sheet. Atmos. Chem. Phys. 13 (9), 4815–4828. https://doi.org/10.5194/acp-13-4815-2013.
Sutanto, S.J., van den Hurk, B., Dirmeyer, P.A., Seneviratne, S.I., Röckmann, T., Trenberth, K.E., Blyth, E.M., Wenninger, J., Hoffmann, G., 2014. HESS opinions "A perspective on isotope versus non-isotope approaches to determine the contribution of transpiration to total evaporation". Hydrol. Earth Syst. Sc. 18, 2815–2827. https://doi.org/10.5194/hess-18-2815-2014.
Wang, K.C., Dickinson, R.E., 2012. A review of global terrestrial evapotranspiration: observation, modeling, climatology, and climatic variability. Rev. Geophys. 50 (2) https://doi.org/10.1029/2011rg000373.
Wang, L., Caylor, K.K., Villegas, J.C., Barron-Gafford, G.A., Breshears, D.D., Huxman, T. E., 2010. Partitioning evapotranspiration across gradients of woody plant cover: Assessment of a stable isotope technique: isotopic evapotranspiration partitioning. Geophys. Res. Lett. 37 (9).
Wang, L.X., Good, S.P., Caylor, K.K., Cernusak, L.A., 2012. Direct quantification of leaf transpiration isotopic composition. Agric. For. Meteorol. 154–155, 127–135. https://doi.org/10.1016/j.agrformet.2011.10.018.
Wang, L.X., Niu, S.L., Good, S.P., Soderberg, K., McCabe, M.F., Sherry, R.A., Luo, Y.Q., Zhou, X.H., Xia, J.Y., Caylor, K.K., 2013. The effect of warming on grassland evapotranspiration partitioning using laser-based isotope monitoring techniques. Geochim. Cosmochim. Acta 111, 28–38. https://doi.org/10.1016/j.gca.2012.12.047.
Wang, L.X., Good, S.P., Caylor, K.K., 2014. Global synthesis of vegetation control on evapotranspiration partitioning. Geophys. Res. Lett. 41 (19), 6753–6757. https://doi.org/10.1002/2014gl061439.

Wang-Erlandsson, L., van der Ent, R.J., Gordon, L.J., Savenije, H.H.G., 2014. Contrasting roles of interception and transpiration in the hydrological cycle—part 1: temporal characteristics over land. Earth Syst. Dynam. 5 (2), 441–469. https://doi.org/10.5194/esd-5-441-2014.

Wen, X.F., Yang, B., Sun, X.M., Lee, X.H., 2016. Evapotranspiration partitioning through in-situ oxygen isotope measurements in an oasis cropland. Agric. For. Meteorol. 230–231, 89–96. https://doi.org/10.1016/j.agrformet.2015.12.003.

Wei, Z.W., Lee, X.H., Wen, X.F., Xiao, W., 2018. Evapotranspiration partitioning for three agri-ecosystems with contrasting moisture conditions: a comparison of an isotope method and a two-source model calculation. Agric. For. Meteorol. 252, 296–310. https://doi.org/10.1016/j.agrformet.2018.01.019.

Wei, Z.W., Yoshimura, K., Okazaki, A., Kim, W., Liu, Z.F., Yokoi, M., 2015. Partitioning of evapotranspiration using high-frequency water vapor isotopic measurement over a rice paddy field. Water Resour. Res. 51 (5), 3716–3729. https://doi.org/10.1002/2014WR016737.

Wei, Z.W., Yoshimura, K., Wang, L.X., Miralles, D.G., Jasechko, S., Lee, X.H., 2017. Revisiting the contribution of transpiration to global terrestrial evapotranspiration. Geophys. Res. Lett. 44, 2792–2801. https://doi.org/10.1002/2016GL072235.

Xiao, W., Lee, X.H., Wen, X.F., Sun, X.M., Zhang, S.C., 2012. Modeling biophysical controls on canopy foliage water $^{18}O$ enrichment in wheat and corn. Glob. Change Biol. 18 (5), 1769–1780. https://doi.org/10.1111/j.1365-2486.2012.02648.x.

Xiao, W., Wei, Z.W., Wen, X.F., 2018. Evapotranspiration partitioning at the ecosystem scale using the stable isotope method—A review. Agric. For. Meteorol. 263, 346–361. https://doi.org/10.1016/j.agrformet.2018.09.005.

Williams, D.G., Cable, W., Hultine, K., Hoedjes, J.C.B., Yepez, E.A., Simonneaux, V., Er-Raki, S., Boulet, G., De Bruin, H.A.R., Chehbouni, A., Hartogensisc, O.K., Timouka, F., 2004. Evapotranspiration components determined by stable isotope, sap flow and eddy covariance techniques. Agric. For. Meteorol. 125 (3), 241–258. https://doi.org/10.1016/j.agrformet.2004.04.008.

Wilson, K.B., Hanson, P.J., Mulholland, P.J., Baldocchi, D.D., Wullschleger, S.D., 2001. A comparison of methods for determining forest evapotranspiration and its components: sap-flow, soil water budget, eddy covariance and catchment water balance. Agric. For. Meteorol. 106 (2), 153–166. https://doi.org/10.1016/s0168-1923(00)00199-4.

Xu, X.J., Zhou, G.M., Liu, S.G., Du, H.Q., Mo, L.F., Shi, Y.J., Jiang, H., Zhou, Y.F., Liu, E. B., 2013. Implications of ice storm damages on the water and carbon cycle of bamboo forests in southeastern China. Agric. For. Meteorol. 177, 35–45. https://doi.org/10.1016/j.agrformet.2013.04.005.

Yakir, D., Sternberg, L.D.L., 2000. The use of stable isotopes to study ecosystem gas exchange. Oecologia 123 (3), 297–311. https://doi.org/10.1007/s004420051016.

Yepez, E.A., Williams, D.G., Scott, R.L., Lin, G.H., 2003. Partitioning overstory and understory evapotranspiration in a semiarid savanna woodland from the isotopic composition of water vapor. Agric. For. Meteorol. 119 (1), 53–68. https://doi.org/10.1016/s0168-1923(03)00116-3.

Zhang, S.C., Wen, X.F., Wang, J.L., Yu, G.R., Sun, X.M., 2010. The use of stable isotopes to partition evapotranspiration fluxes into evaporation and transpiration. Acta Ecologica Sinica. 30 (4), 201–209. https://doi.org/10.1016/j.chnaes.2010.06.003.

Zhang, S., Zhang, J., Liu, B.o., Zhang, W., Gong, C., Jiang, M., Lv, X., 2018. Evapotranspiration partitioning using a simple isotope-based model in a semiarid marsh wetland in northeastern China. Hydrol. Process. 32 (4), 493–506.

Zhang, Y.C., Shen, Y.J., Sun, H.Y., Gates, J.B., 2011. Evapotranspiration and its partitioning in an irrigated winter wheat field: a combined isotopic and micro-meteorologic approach. J. Hydrol. 408 (3–4), 203–211. https://doi.org/10.1016/j.jhydrol.2011.07.036.

Zhou, S., Yu, B.F., Zhang, Y., Huang, Y.F., Wang, G.Q., 2016. Partitioning evapotranspiration based on the concept of underlying water use efficiency. Water Resour. Res. 52 (2), 1160–1175. https://doi.org/10.1002/2015WR017766.

Zhu, G.F., Su, Y.H., Li, X., Zhang, K., Li, C.B., 2013. Estimating actual evapotranspiration from an alpine grassland on Qinghai-Tibetan plateau using a two-source model and parameter uncertainty analysis by Bayesian approach. J. Hydrol. 476 (7), 42–51. https://doi.org/10.1016/j.jhydrol.2012.10.006.

Zimmermann, U., Ehhalt, D., Münnich, K.O., 1967. Soil-water movement and evapotranspiration: changes in the isotopic composition of the water. In: Proceedings of the Symposium of Isotopes in Hydrology, pp. 567–584.